(Received 11 September 2025, Accepted 15 October 2025, Scheduled 28 October 2025)

Compact Substrate-Integrated Waveguide Bandpass Filter Using Open-Circuited and Short-Circuited Vias and Slots

Qun-Lin Chen and Chun-Long Wang*

National Taiwan University of Science and Technology, Taipei 106335, Taiwan

ABSTRACT: This paper presents a compact substrate-integrated waveguide (SIW) bandpass filter featuring a simple structure and transmission zeros. The proposed filter utilizes a quarter-wavelength transmission line in conjunction with a short-circuited and open-circuited via structure to achieve a third-order bandpass filter response. The filter achieves a passband from 14.15 GHz to 15.86 GHz with a return loss ($|S_{11}|$) better than -10 dB, indicating good impedance matching. To enhance out-of-band rejection, single- and double-slot structures are introduced along the quarter-wavelength transmission line of the SIW filter without increasing the overall circuit area. The SIW filter using the single-slot structure generates a transmission zero at 16.5 GHz, albeit with limited suppression. In contrast, the SIW filter using the double-slot structure introduces a deeper transmission zero at the same frequency, substantially improving stopband attenuation while maintaining excellent passband performance. The proposed filter offers high selectivity, compact size, and structural simplicity, making it a strong candidate for high-frequency communication and radar system applications. To validate the design, prototypes of the SIW bandpass filter, including the prototype version, single-slot version, and double-slot version, were fabricated and measured. The measurement results show good agreement with the simulation results.

1. INTRODUCTION

Waveguide technology was first proposed by J. J. Thomson in 1893 [1–3]. Due to its low transmission loss and high power-handling capability, it has been widely employed in high-frequency and long-distance systems. However, waveguides are typically bulky, costly, and difficult to fabricate, which limits their applicability in modern electronic systems. The emergence of planar transmission line technology in the 1960s revolutionized microwave circuit design. Planar transmission lines, such as microstrip lines [4], coplanar waveguides (CPWs) [5], and slotlines [6], offer advantages including compact size, light weight, ease of fabrication, and compatibility with integrated circuits. These features have led to their widespread adoption in monolithic microwave integrated circuits (MMICs) and microwave integrated circuits (MICs).

To combine the advantages of waveguides and planar transmission lines, the concept of the substrate-integrated waveguide (SIW) was introduced in 1998 [7]. It was further advanced by Deslandes and Wu in 2001 through its implementation using standard printed circuit board (PCB) processes [8]. SIW preserves the high-Q factor and low-loss characteristics of metallic waveguides while significantly reducing size and fabrication costs. Moreover, SIW circuits can be seamlessly integrated with other planar transmission lines and components, making them attractive for compact system-on-substrate implementations.

SIW technology has been widely adopted in high-frequency filter design, and numerous SIW-based bandpass filter designs have been reported in the literature. For example, an SIW dual-band filter using symmetric coupling slots was presented in [9], achieving a passband between 14.76 GHz and 16.78 GHz with low insertion and return loss. This approach was later extended to a triple-band design by etching defected ground structures (DGSs) and defected microstrip structures (DMSs) onto the top and bottom metallization layers [10]. To achieve miniaturization, a slow-wave structure was employed to reduce the size of the SIW cavity by 40% [11]. Further size reduction was achieved by transforming a single-layer third-order SIW filter into a folded three-layer structure, resulting in a fivefold reduction in longitudinal dimension with only a twofold increase in height [12].

To support accurate SIW filter modeling, Goldfarb and Pucel proposed an equivalent circuit theory based on microstrip via-hole modeling, which enabled precise *LC* representation and control of transmission zeros [13]. Building upon this foundation, mushroom-shaped resonators were introduced to generate additional transmission zeros, thereby enhancing out-of-band suppression [14]. In [15], a partially plated via was employed to achieve stopband attenuation up to 60 dB. A symmetrical DGS slot was also utilized to broaden the filter bandwidth while introducing a transmission zero [16]. Other advancements include the integration of complementary split ring resonators (CSRRs) [17], the application of spiral resonators for dual stopbands in the Ka/V-band [18], and the use of back-to-back *E*-type DGS combined with double-sided loading structures to generate controllable transmission poles and zeros within a compact footprint [19].

While these prior works have achieved substantial improvements in filter performance, most rely on short-circuit vias to

* Corresponding author: Chun-Long Wang (clw@mail.ntust.edu.tw).

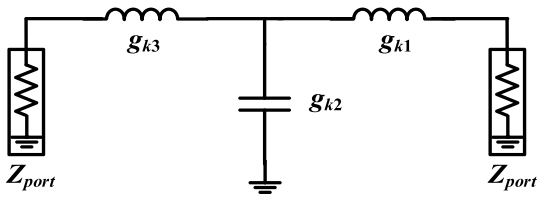

FIGURE 1. Low-pass filter prototype.

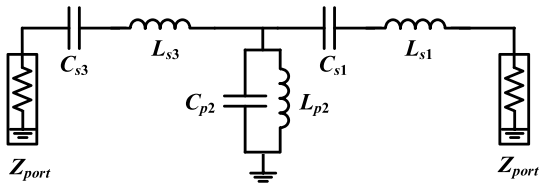

FIGURE 2. Bandpass filter prototype.

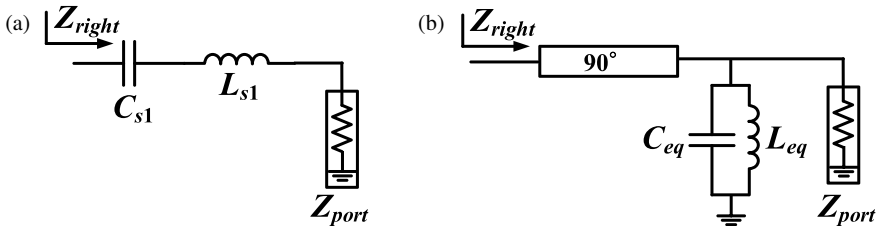

FIGURE 3. Transformation between series and parallel LC resonators. (a) Series LC resonator. (b) Parallel LC resonator.

form resonant cavities, or employ slot structures to introduce transmission zeros, precise control over the location of these transmission zeros and the overall filter response remains a challenge, especially under constraints of miniaturization and fabrication simplicity.

To address these limitations, this paper proposes a novel SIW bandpass filter that utilizes a combination of short- and open-circuited vias to realize a third-order bandpass filter response. Additionally, single- and double-slot structures are incorporated to generate transmission zeros without increasing the circuit footprint. The proposed design is compact and straightforward, composed solely of vias and slots, yet capable of delivering enhanced frequency selectivity and stopband attenuation.

The remainder of this paper is organized as follows. Section 2 presents the design and analysis of the SIW bandpass filter using short- and open-circuited vias. Section 3 introduces a single-slot SIW bandpass filter using short- and open-circuited vias and examines its transmission zero characteristics. Section 4 extends the design to a double-slot SIW bandpass filter using the short- and open-circuited vias, demonstrating improved out-of-band rejection. Finally, Section 5 concludes the paper with a summary of the proposed approach and its potential applications.

2. SIW BANDPASS FILTER USING SHORT- AND OPEN-CIRCUITED VIAS

This section describes the design method for a substrate-integrated waveguide (SIW) bandpass filter using short- and open-circuited vias. The characteristic impedance of the filter system is set to $Z_{port} = 58.92\,\Omega$. The filter's center frequency is set to $f_0 = 15\,\text{GHz}$, targeting Ku-band applications. A fractional bandwidth of 10% is selected, corresponding to an absolute bandwidth of $\Delta f = 1.5\,\text{GHz}$. The filter's order is designed to be $N = 3$, with a passband ripple of 0.5 dB to achieve the desired Chebyshev response. The filter is implemented using a Rogers® RO4003 substrate with a relative permittivity of $\varepsilon_r = 3.55$, a substrate thickness of 1.52 mm, a conductor thickness of 35 µm, and a loss tangent of 0.0027.

2.1. Equivalent Circuit

Given the specifications of the bandpass filter: center frequency $f_0 = 15\,\text{GHz}$, fractional bandwidth of 10%, order $N = 3$, and passband ripple of 0.5 dB, the lowpass prototype component values can be obtained from the Chebyshev filter design table [19]. These values are $g_{k1} = g_{k3} = 1.5963$ and $g_{k2} = 1.0967$ with the lowpass prototype filter shown in Fig. 1. By applying the lowpass to bandpass transformation, the lowpass filter prototype in Fig. 1 can be converted to the bandpass filter prototype shown in Fig. 2. In this transformation, g_{k1} and g_{k3} are converted to series LC resonators, while g_{k2} is converted to a parallel LC resonator. The inductor and capacitor values of these LC resonators are calculated as follows: $L_{s1}(L_{s3}) = 9.98\,\text{nH}$, $C_{s1}(C_{s3}) = 0.0113\,\text{pF}$, $L_{p2} = 0.057\,\text{nH}$, $C_{p2} = 1.975\,\text{pF}$.

In SIW structures, as parallel LC resonators can be easily implemented through short- and open-circuited vias, series LC resonators should be transformed into parallel LC resonators. Therefore, this design uses a quarter-wavelength transmission line to convert the first and third series LC resonators into parallel LC resonators. The equivalent transformation circuit is illustrated in Fig. 3. By ensuring that input impedances of the two circuits are equal, the relationship between the inductance and capacitance of the two configurations can be derived, as shown in Equations (1) and (2). Substituting $L_{s1}(L_{s3}) = 9.98\,\text{nH}$, $C_{s1}(C_{s3}) = 0.0113\,\text{pF}$, $Z_{port} = 58.92\,\Omega$ into Equations (1) and (2), the equivalent transformed inductance and capacitance values are $L_{eq} = 0.03923\,\text{nH}$ and $C_{eq} = 2.875\,\text{pF}$.

$$L_{eq} = Z_{port}^2 C_{s1} \tag{1}$$

$$C_{eq} = \frac{L_{s1}}{Z_{port}^2} \tag{2}$$

By replacing the series LC resonator in the bandpass filter prototype in Fig. 2 with the equivalent parallel LC resonator and the quarter-wavelength transmission line shown in Fig. 3, a transformed bandpass filter prototype is obtained, as shown in Fig. 4. To verify that the transformed bandpass filter prototype

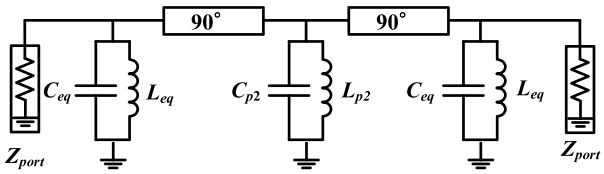

FIGURE 4. Transformed bandpass filter prototype.

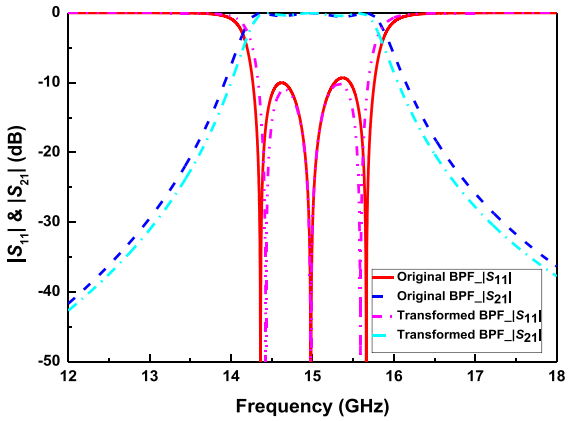

FIGURE 5. Frequency responses of the reflection and transmission coefficients for the original and transformed bandpass filter prototypes.

in Fig. 4 is functionally equivalent to the original bandpass filter prototype in Fig. 2, both circuits were simulated using the Advanced Design System (ADS). Fig. 5 shows the frequency responses of the reflection and transmission coefficients of the two designs. As can be seen in Fig. 5, frequency responses of the original and transformed bandpass filter prototypes agree well, demonstrating the accuracy and effectiveness of the transformation using a quarter-wavelength transmission line.

2.2. Circuit Implementation and Analysis

2.2.1. Quarter-Wavelength SIW

The quarter-wavelength transmission line of the transformed bandpass filter prototype in Fig. 4 will now be realized with a quarter-wavelength SIW in Fig. 6. The quarter-wavelength SIW will be implemented on a Rogers® RO4003 substrate with a relative dielectric constant of $\varepsilon_r = 3.55$, a substrate thickness of $h = 1.5$ mm, a conductor thickness of 35 µm, and a characteristic impedance of $Z_{port} = 58.92\,\Omega$. To prevent leakage from the SIW cavity sidewall vias and improve wave confinement, the via diameter was designed to be $d = 0.82$ mm, and the via pitch was designed to be $p = 1.1$ mm [9, 10]. To ensure good reflection and transmission characteristics within the operating frequency band (12–18 GHz), the cutoff frequency f_c of the TE_{10} mode was set to 10.26 GHz, resulting in an effective SIW width of $W_{SIW} = 8.4$ mm. To determine the length of the quarter-wavelength SIW shown in Fig. 6, a phase simulation was performed, and the simulated frequency response of the phase is shown in Fig. 7. When the SIW length is set to $L_{SIW} = 4.15$ mm, the phase at 15 GHz is 89.9°, consistent with the theoretical quarter-wavelength value of 90°. Furthermore,

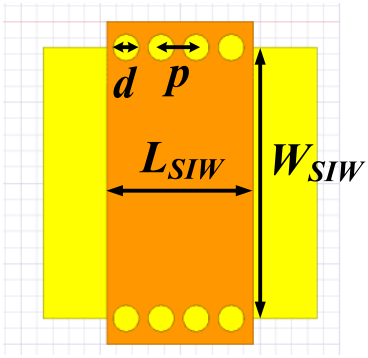

FIGURE 6. The quarter-wavelength SIW structure.

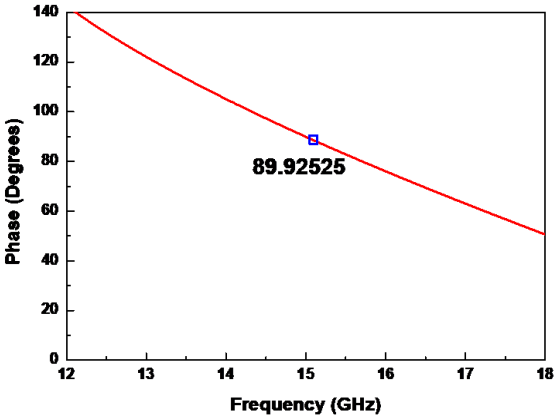

FIGURE 7. Frequency response of the phase for the quarter-wavelength SIW structure.

the port impedance Z_{pi} of SIW obtained through simulation confirms that the SIW impedance at 15 GHz is $Z_{port} = 58.92\,\Omega$.

2.2.2. First and Third LC Resonators

Reconsidering the transformed bandpass filter prototype in Fig. 4, the first and third parallel LC resonators are identical. Their equivalent inductance and capacitance values are $L_{eq} = 0.03923$ nH and $C_{eq} = 2.875$ pF, respectively. Since the first and third parallel LC resonators are identical, only the first LC parallel resonator needs to be considered, and the results will be applied to the third LC parallel resonator. The inductance of the first parallel LC resonator can be implemented using a short-circuited via connecting the top and bottom metal layers, as shown in Fig. 8. By simulating the short-circuited via in Fig. 8(a) with a via diameter of $D_{via} = 1.53$ mm and the equivalent inductance in Fig. 8(b) with an inductance value of $L_{via} = L_{eq} = 0.03923$ nH, the frequency responses of the reflection and transmission coefficients are shown in Fig. 9. The frequency responses of reflection and transmission coefficients for these two models show good agreement, indicating that the short-circuited via structure provides the required inductance at 15 GHz.

To realize the equivalent capacitance of $C_{eq} = 2.875$ pF, two open-circuited vias were designed. The open-circuited via is connected to the top metal layer, while a coaxially removed annular region is provided in the lower ground layer,

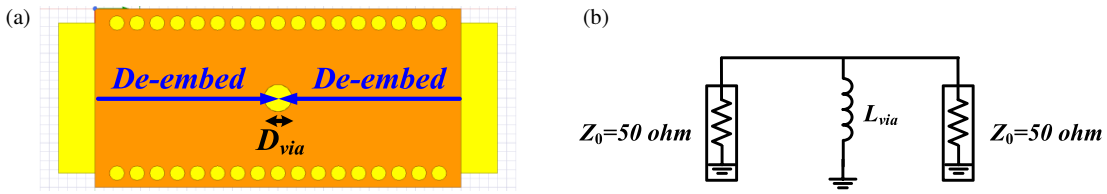

FIGURE 8. Short-circuited via and its equivalent inductance. (a) Short-circuited via. (b) Equivalent inductance.

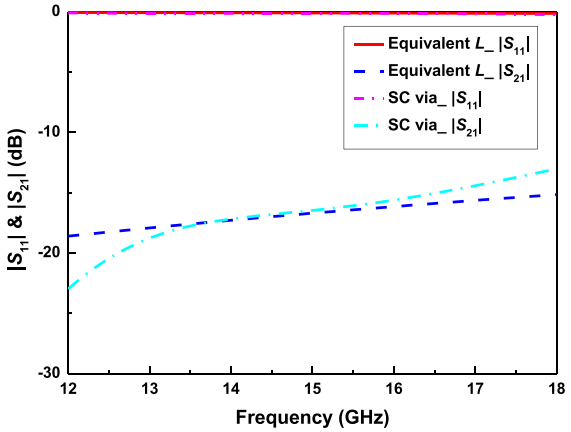

FIGURE 9. Frequency responses of the reflection and transmission coefficients for the short-circuited via and its equivalent inductance.

leaving the via open-circuited at ground, creating a capacitive effect, as shown in Fig. 10(a). However, this structure also introduces a parasitic inductance, forming a parallel LC circuit as shown in Fig. 10(b). The diameter of the open-circuited via is $D_{via} = 1.53$ mm, and the ground removal gap is $G = 0.06$ mm. The value of the parasitic inductance is $L_p = 0.06399$ nH, and the value of the equivalent capacitance is $C_{via} = C_{eq} = 2.875$ pF. To verify the equivalence of the two circuits, a High Frequency Structure Simulator (HFSS) simulation was performed on the open-circuited via in Fig. 10(a), and an ADS simulation was performed on the equivalent inductance and capacitance in Fig. 10(b). The frequency responses of the reflection and transmission coefficients are shown in Fig. 11, confirming that the open-circuited via structure can be well represented by the parallel LC circuit.

To realize the first parallel LC resonator of the transformed bandpass filter prototype in Fig. 4, the short-circuited via in Fig. 8(a) and the open-circuited vias in Fig. 10(a) are combined as shown in Fig. 12(a). The diameter of the open-circuited via is $D_{via} = 1.53$ mm, and the ground removal gap is $G = 0.06$ mm. As the open-circuited vias in Fig. 10(a) will introduce a parasitic inductance of $L_p = 0.06399$ nH, the resonant frequency of the short-circuited combined with the open-circuited vias in Fig. 12(a) will shift downward to approximately 12.4 GHz. To compensate for the influence of the parasitic inductance $L_p = 0.06399$ nH, the diameter of the open-circuited via D_{via} and ground removal gap G are optimized. As the parasitic inductance L_p is associated with open-circuited vias, the ground removal gap G should be substantially optimized to alleviate the influence of parasitic inductance L_p. As the effect of parasitic inductance L_p is alleviated, the diameter of short-circuited via D_{via}, which is the same as the diameter of open-circuited via D_{via}, should be slightly optimized to compensate for the influence of alleviated parasitic inductance L_p. The optimized diameter of the open-circuited via is $D_{via} = 14$ mm, and the optimized ground removal gap is $G = 0.17$ mm. HFSS simulations were performed on the short-circuited combined with the open-circuited vias in Fig. 12(a), and ADS simulations were performed on the equivalent inductance and capacitance circuit in Fig. 12(b) with $L_{via} = L_{eq} = 0.03923$ nH and $C_{via} = C_{eq} = 2.875$ pF. The frequency responses of the reflection and transmission coefficients for the short-circuited combined with open-circuited vias and their equivalent inductance and capacitance are shown in Fig. 13. The high degree of consistency of the results verifies the accuracy and feasibility of the design.

2.2.3. Second LC Resonator

Reconsidering the transformed bandpass filter prototype in Fig. 4, we will now discuss the design of the second parallel LC resonator. While the structure of the second parallel LC resonator is the same as the structures of the first and third parallel LC resonators, the resonator parameters are different, requiring redesign of the via and gap geometry to meet specific requirements. The inductance and capacitance of the second parallel LC resonator are $L_{p2} = 0.057$ nH and $C_{p2} = 1.975$ pF, respectively. The inductance of the second parallel LC resonator can be implemented using a short-circuited via connecting the top and bottom metal layers, as shown in Fig. 8. By simulating the short-circuited via in Fig. 8(a) with a via diameter of $D_{via} = 1.28$ mm and the equivalent inductance in Fig. 8(b) with an inductance value of $L_{via} = L_{p2} = 0.057$ nH, the frequency responses of the reflection and transmission coefficients are shown in Fig. 14. The frequency responses of the reflection and transmission coefficients for these two models show good agreement, indicating that the short-circuited via structure provides the required inductance at 15 GHz.

To realize the capacitance of $C_{p2} = 1.975$ pF, two open-circuited vias were designed. The open-circuited via is connected to the top metal layer, while a coaxially removed annular region is provided in the lower ground layer, leaving the via open-circuited at ground, creating a capacitive effect, as shown in Fig. 10(a). However, this structure also introduces a parasitic inductance, forming a parallel LC circuit as shown in Fig. 10(b). The diameter of the open-circuited via is $D_{via} = 1.28$ mm, and the ground removal gap is $G = 0.08$ mm. The value of the parasitic inductance is $L_p = 0.0944$ nH, and the value of the equivalent capacitance is $C_{via} = C_{p2} = 1.975$ pF. To verify the equivalence of the two circuits, an HFSS simulation was performed on the open-circuited via in Fig. 10(a), and an ADS sim-

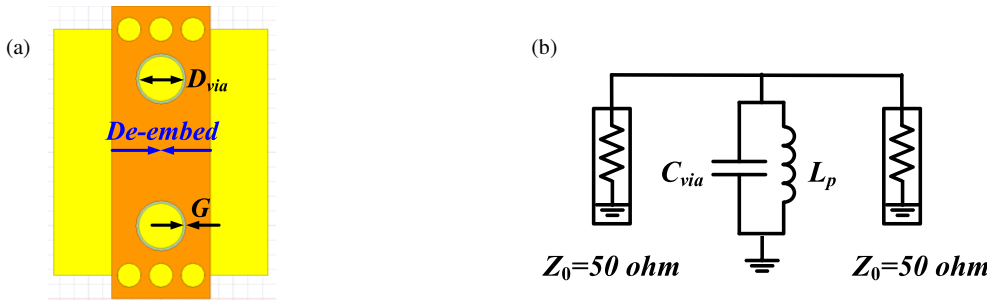

FIGURE 10. Open-circuited via and its equivalent inductance and capacitance. (a) Open-circuited via. (b) Equivalent inductance and capacitance.

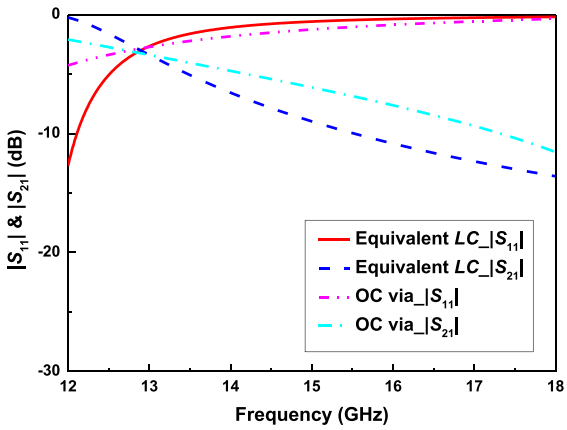

FIGURE 11. Frequency responses of the reflection and transmission coefficients for the open-circuited via and its equivalent inductance and capacitance.

ulation was performed on the equivalent inductance and capacitance in Fig. 10(b). The frequency responses of the reflection and transmission coefficients are shown in Fig. 15, confirming that the open-circuited via structure can be well represented by the parallel LC circuit.

To realize the second parallel LC resonator of the transformed bandpass filter prototype in Fig. 4, the short-circuited via in Fig. 8(a) and the open-circuited vias in Fig. 10(a) are combined as shown in Fig. 12(a). The diameter of the open-circuited via is $D_{via} = 1.28$ mm, and the ground removal gap is $G = 0.08$ mm. As the open-circuited vias in Fig. 10(a) will introduce a parasitic inductance of $L_p = 0.08583$ nH, the resonant frequency of the short-circuited combined with the open-circuited vias in Fig. 12(a) will shift downward to approximately 12.4 GHz. To compensate for the influence of the parasitic inductance $L_p = 0.08583$ nH, the diameter of the open-circuited via D_{via} and ground removal gap G are optimized. As the parasitic inductance L_p is associated with the open-circuited vias, the ground removal gap G should be substantially optimized to alleviate the influence of parasitic inductance L_p. As the effect of parasitic inductance L_p is alleviated, the diameter of short-circuited via D_{via}, which is the same as the diameter of open-circuited via D_{via}, should be slightly optimized to compensate for the influence of alleviated parasitic inductance L_p. The optimized diameter of the open-circuited via is $D_{via} = 1.24$ mm, and the optimized ground removal gap is $G = 0.19$ mm. HFSS simulations were performed on the short-circuited combined with the open-circuited vias in Fig. 12(a), and ADS simulations were performed on the equivalent inductance and capacitance circuit in Fig. 12(b) with $L_{via} = L_{p2} = 0.057$ nH and $C_{via} = C_{p2} = 1.975$ pF. The frequency responses of the reflection and transmission coefficients for the short-circuited combined with open-circuited vias and their equivalent inductance and capacitance are shown in Fig. 16. The high degree of consistency of the results verifies the accuracy and feasibility of the design.

2.2.4. Characteristic Impedance Z_{port}

To realize the characteristic impedance $Z_{port} = 58.92\,\Omega$, an impedance matching structure was designed. The impedance matching structure consists of a section of 58.92-Ω SIW in series with a section of 50-Ω microstrip line, as shown in Fig. 17. Impedance matching was achieved when the section of 58.92-Ω SIW length was set to 1.95 mm. To verify the matching performance, an HFSS simulation was performed, with the SIW port deembedded to the position of the first parallel LC resonator and the input impedance Z_{in} observed in this direction. At 15 GHz, the input impedance Z_{in} was approximately 59.6 Ω, which is close to the characteristic impedance $Z_{port} = 58.92\,\Omega$, confirming that the matching structure met the design objectives.

2.2.5. Third-Order SIW Bandpass Filter

By replacing the 90° transmission line in Fig. 4 with the quarter-wavelength SIW structure shown in Fig. 6, the parallel LC resonator in Fig. 4 with the short-circuited via with the open-circuited via structure shown in Fig. 12, and the characteristic impedance $Z_{port} = 58.92\,\Omega$ with the 58.92-Ω SIW in series with 50-Ω microstrip line shown in Fig. 17, a SIW bandpass filter using the short- and open-circuited vias can be formed as shown in Fig. 18. The SIW bandpass filter using the short- and open-circuited vias in Fig. 18 was simulated using HFSS, and the frequency responses of simulated reflection and transmission coefficients are shown in Fig. 19. This filter has a passband range of 14.15 GHz to 15.86 GHz, with a reflection coefficient $|S_{11}|$ below -10 dB throughout the entire passband, demonstrating good passband characteristics and impedance matching. However, parasitic effects in the actual structure can cause slight differences between the HFSS and equivalent circuit responses, requiring further design fine-tuning. To compensate for this effect, the via diameters and gap spacing of the three res-

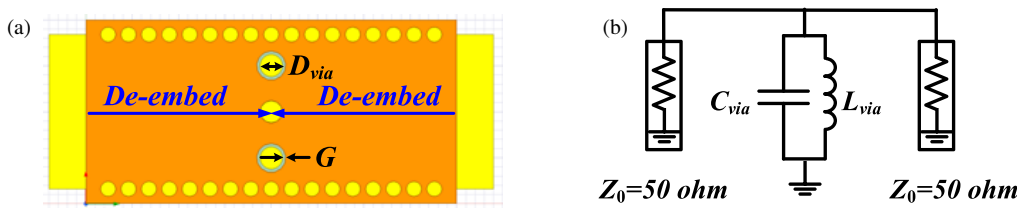

FIGURE 12. Short-circuited combined with open-circuited vias and their equivalent inductance and capacitance. (a) Short-circuited combined with open-circuited vias. (b) Equivalent inductance and capacitance.

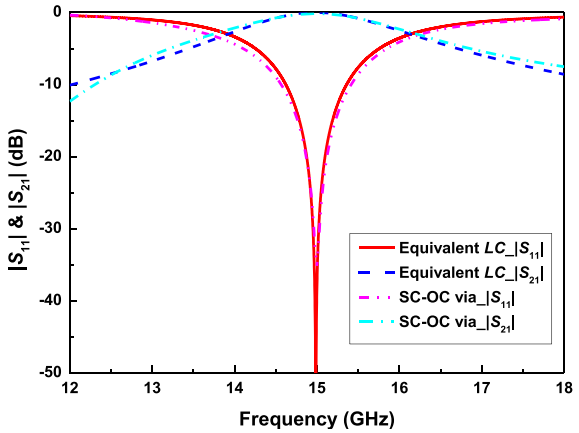

FIGURE 13. Frequency responses of the reflection and transmission coefficients for the short-circuited combined with open-circuited vias and their equivalent inductance and capacitance.

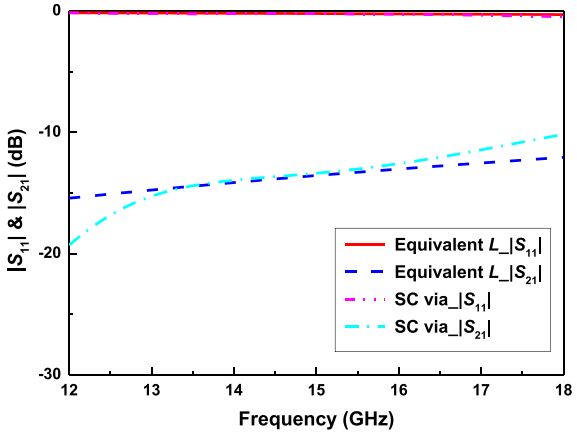

FIGURE 14. Frequency responses of the reflection and transmission coefficients for the short-circuit via and its equivalent inductance.

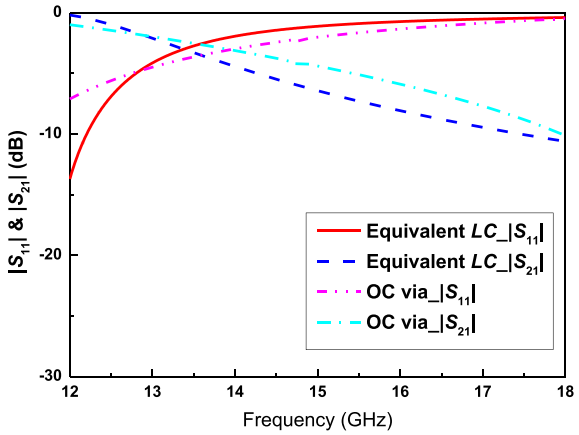

FIGURE 15. Frequency responses of the reflection and transmission coefficients for the open-circuit via and its equivalent inductance and capacitance.

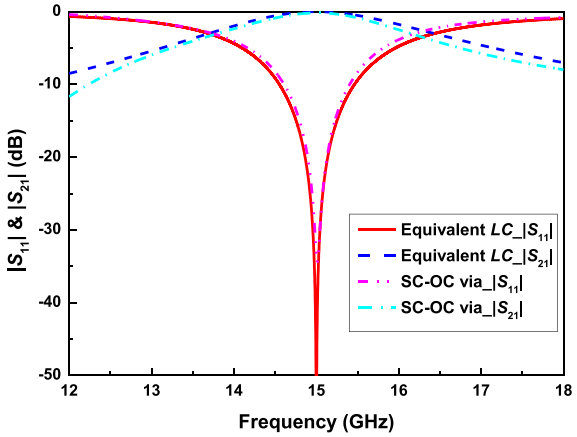

FIGURE 16. Frequency responses of the reflection and transmission coefficients for the short-circuited combined with open-circuited vias and their equivalent inductance and capacitance.

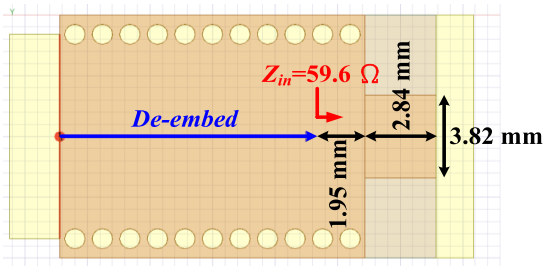

FIGURE 17. A series connection of a section of 58.92-Ω SIW and a 50-Ω microstrip line.

onant cavities were optimized. The optimized dimensions are listed in Table 1, and the updated simulation results are shown in Fig. 19. The deviated center frequency at 15.2 GHz has been corrected back to 15 GHz, eliminating the passband offset.

2.2.6. Implementation and Measurement Results

To verify the performance of the SIW bandpass filter using the short- and open-circuited vias, the SIW bandpass filter using the short- and open-circuited vias shown in Fig. 18 was fabricated as shown in Fig. 20. To facilitate the measurement, SMA connectors were soldered to the input/output microstrip

TABLE 1. Dimensions of the SIW bandpass filter using the short- and open-circuited vias before and after optimization.

	$D_{via(left,right)}$	$G_{(left,right)}$	$D_{via(mid)}$	$G_{(mid)}$	d
Original	1.4	0.17	1.24	0.19	4.15
Optimized	1.17	0.19	1.21	0.185	4.15

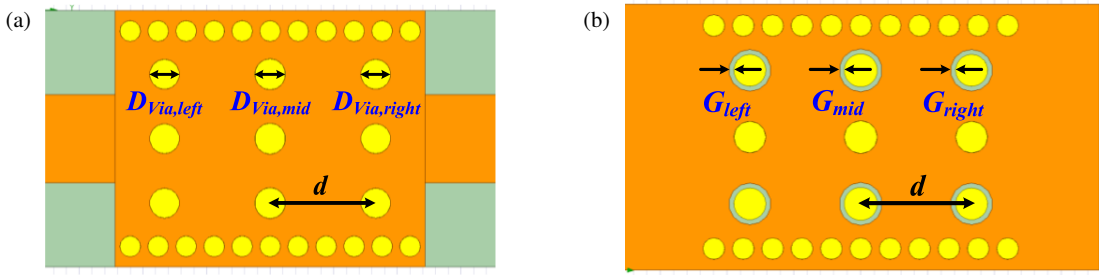

FIGURE 18. The SIW bandpass filter using the short- and open-circuited vias. (a) Top view. (b) Bottom view.

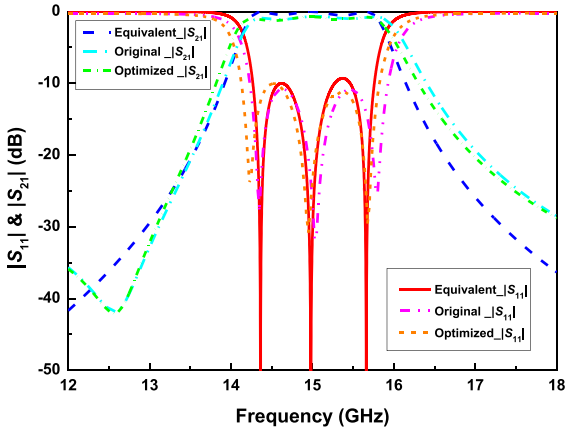

FIGURE 19. The frequency responses of the reflection and transmission coefficients for the SIW bandpass filter using the short- and open-circuited vias.

lines. After calibrating the Agilent E5071C vector network analyzer (VNA) using the Keysight 85521A calibration kit, the filter's S-parameters were measured and compared with HFSS simulation results as shown in Fig. 21. As can be seen from Fig. 21, the measurement result agrees well with the simulation one. The measured reflection coefficient $|S_{11}|$ remains below -10 dB within the passband, indicating good impedance matching. The measured transmission coefficient $|S_{21}|$ exhibits the multi-resonance characteristics of a third-order bandpass filter. However, the measured $|S_{21}|$ is slightly lower than the simulated $|S_{21}|$, which is likely due to losses introduced by the SMA connectors.

3. SINGLE-SLOT SIW BANDPASS FILTER USING SHORT- AND OPEN-CIRCUITED VIAS

3.1. Circuit Implementation and Analysis

To implement a filter with a transmission zero, a parallel LC resonator can be cascaded to the transformed bandpass filter prototype shown in Fig. 4, forming a single-zero bandpass filter prototype as shown in Fig. 22. The parallel LC resonator exhibits high impedance at its resonant frequency. When being placed in the main transmission path, it blocks signal propagation, forming a significant transmission zero and enhancing the filter's out-of-band suppression. When the parallel LC resonator has an inductance of $L = 0.01695$ nH and a capacitance of $C = 5.74048$ pF, a transmission zero is generated at 16.2 GHz. To verify the generated transmission zero, the single-zero bandpass filter prototype shown in Fig. 22 is simulated by ADS, and the frequency responses of reflection and transmission coefficients are shown in Fig. 23. This figure clearly shows a significant drop in the transmission coefficient near 16.2 GHz, confirming that the structure successfully creates the desired transmission zero.

The cascaded parallel LC resonator in Fig. 22 can be implemented with a single slot as shown in Fig. 24(a). Its original dimensions are listed in Table 2. HFSS simulations were performed on the single-slot structure in Fig. 24(a), and ADS simulations were performed on the cascaded parallel LC resonator in Fig. 24(b). The frequency responses of reflection and transmission coefficients are shown in Fig. 25. As can be seen from Fig. 25, the simulation results for the single-slot structure closely match those for the cascaded parallel LC circuit resonator, confirming that the single slot structure can effectively represent a cascaded parallel LC resonator.

By integrating the single-slot structure shown in Fig. 24(a) with the SIW bandpass filter using the short- and open-circuited vias shown in Fig. 18, a single-slot SIW bandpass filter using the short- and open-circuited vias can be realized as shown in Fig. 26. The slot is located in the quarter-wavelength SIW portion of the filter, eliminating the need to increase circuit area. However, this combination introduces coupling effects, causing the transmission zero to shift downward from the intended 16.2 GHz to approximately 15.5 GHz. To address this issue, the slot dimensions must be adjusted to shift the transmission zero back to the target frequency of 16.2 GHz. The adjusted dimensions are listed in Table 2. Fig. 27 shows the HFSS sim-

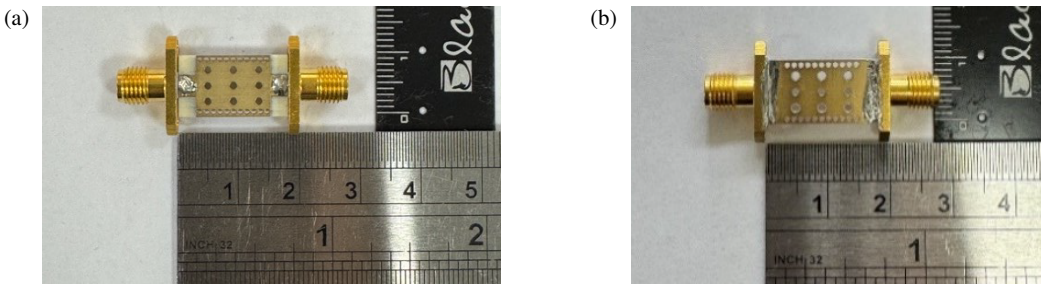

FIGURE 20. Real circuit of the SIW bandpass filter using the short- and open-circuited vias. (a) Top view. (b) Bottom view.

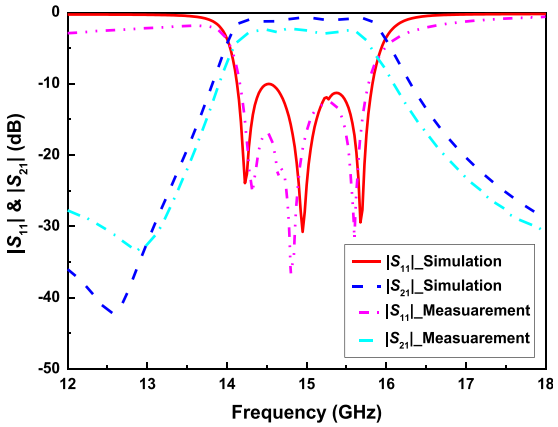

FIGURE 21. Comparison between the simulated and measured frequency responses of the reflection and transmission coefficients for the SIW bandpass filter using the short- and open-circuited vias.

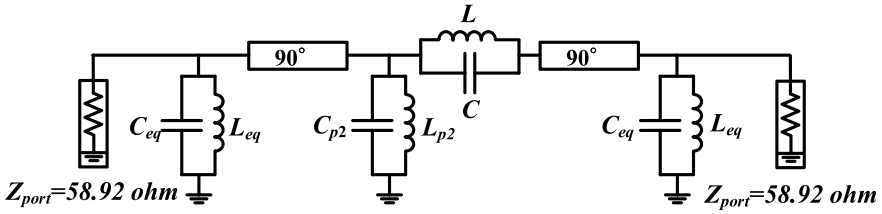

FIGURE 22. The single-zero bandpass filter prototype.

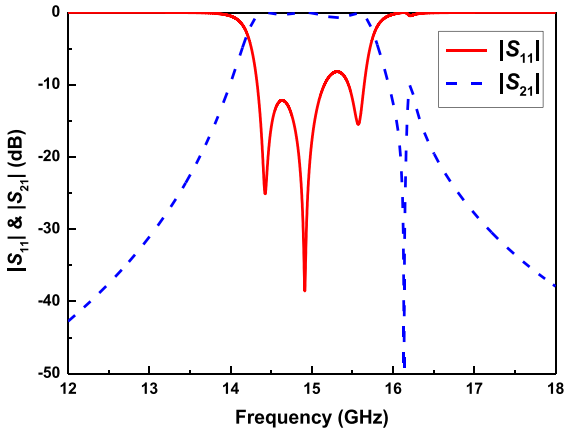

FIGURE 23. The frequency responses of the reflection and transmission coefficients for the single-zero bandpass filter prototype.

ulation results of the single-slot SIW bandpass filter using the short- and open-circuited vias in Fig. 26. The results show good agreement between the physical layout and the equivalent circuit model, with a transmission zero observed at 16.2 GHz where $|S_{21}|$ is below -20 dB.

TABLE 2. Dimensions of the single-slot structure before and after optimization (unit: mm).

	H	*h*	*W*	*w*
Original	**5.33**	**2.7**	**1.76**	**0.3**
Optimized	**5.33**	**2.57**	**1.76**	**0.3**

3.2. Implementation and Measurement Results

To verify the performance of the single-slot SIW bandpass filter using short- and open-circuited vias, the single-slot SIW bandpass filter using the short- and open-circuited vias in Fig. 26 is fabricated as shown in Fig. 28. To facilitate measurement, SMA connectors were soldered to the microstrip input and output ports. An Agilent E5071C vector network analyzer was calibrated using a Keysight 85521A calibration kit. Subsequently, S-parameters of the fabricated filter were measured

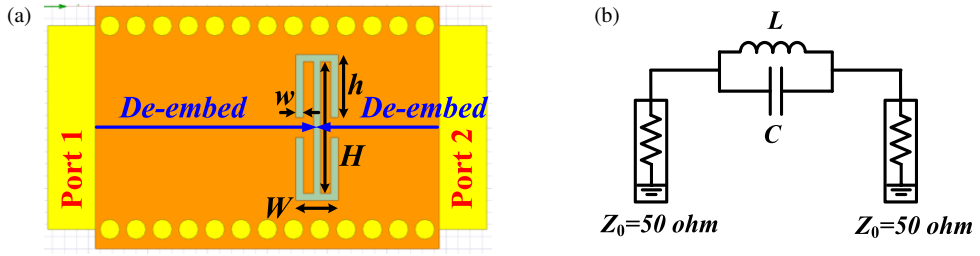

FIGURE 24. Single-slot structure and its equivalent parallel LC resonator. (a) Single-slot structure. (b) Equivalent parallel LC resonator.

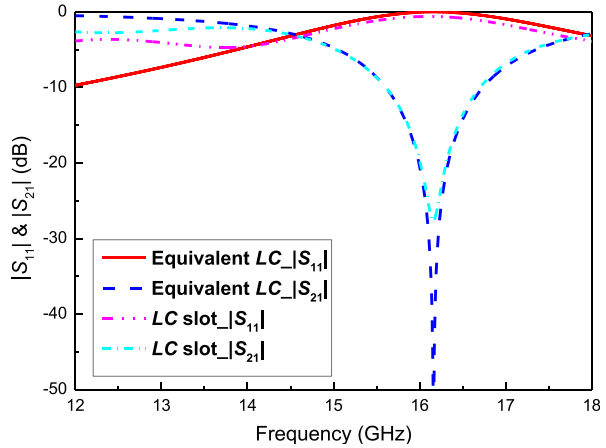

FIGURE 25. The frequency responses of the reflection and transmission coefficients for the single-slot structure and its equivalent parallel LC resonator.

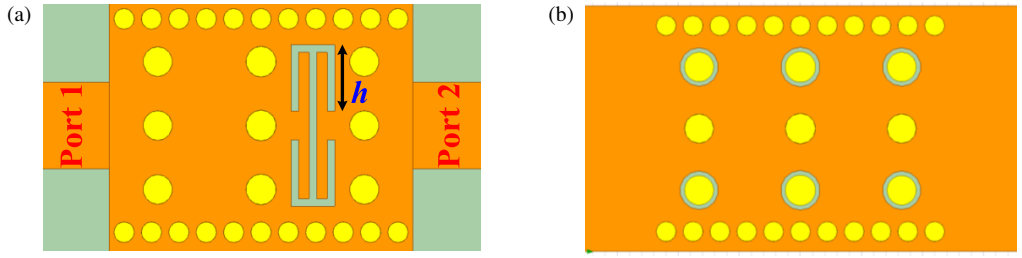

FIGURE 26. Single-slot SIW bandpass filter using the short- and open-circuited vias. (a) Top view. (b) Bottom view.

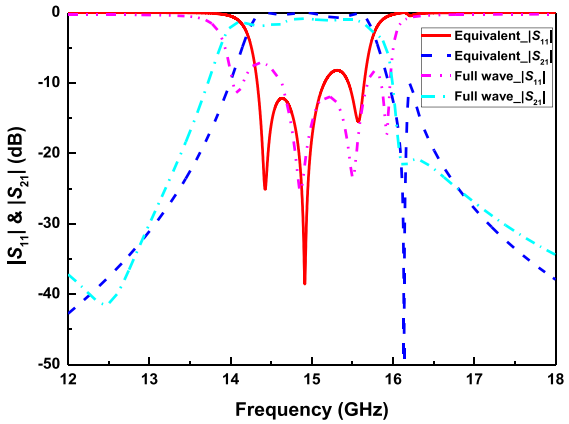

FIGURE 27. Frequency response of the reflection and transmission coefficients for the single-slot SIW bandpass filter using the short- and open-circuited vias.

and compared with HFSS simulation results. A comparison of the simulated and measured frequency responses is shown in Fig. 29. As can be seen from Fig. 29, the overall trends of the measured and simulated frequency responses are well aligned. The measured reflection coefficient $|S_{11}|$ remains below -10 dB within the passband, indicating good impedance matching, while the transmission coefficient $|S_{21}|$ exhibits the expected multi-resonant characteristics of a third-order bandpass filter. However, the measured $|S_{21}|$ is slightly lower than the simulated $|S_{21}|$, which is attributed to the losses introduced by the SMA connectors. The discrepancy between the simulated and measured $|S_{11}|$ within the 14–15 GHz range may be attributed to the imperfect soldering effect of SMA connectors. Regarding the transmission zero, simulations predict a deep notch at 16.2 GHz, while measurements show a slight shift to around 16.5 GHz. The slight deviation is caused by the manufacturing tolerances of the single slot structure.

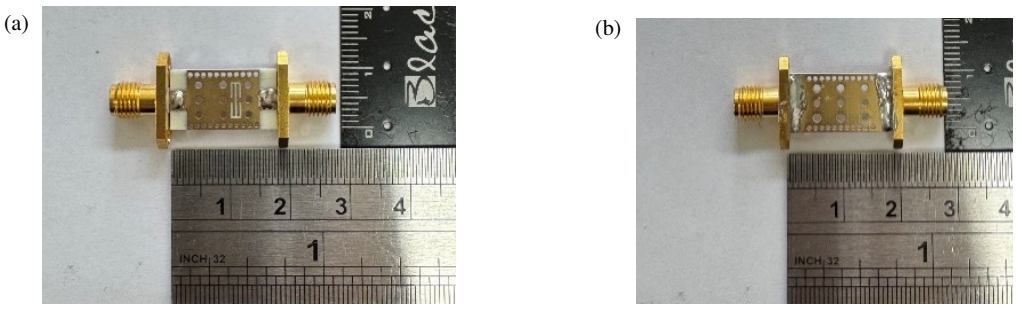

FIGURE 28. Real circuit of the single-slot SIW bandpass filter using the short- and open-circuited vias. (a) Top view. (b) Bottom view.

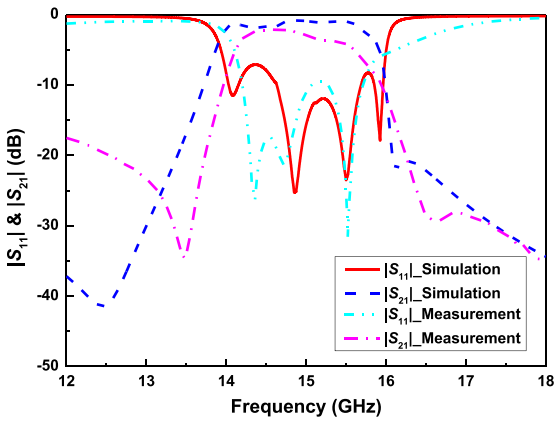

FIGURE 29. Comparison between the simulated and measured frequency responses of the reflection and transmission coefficients for the single-slot SIW bandpass filter using the short- and open-circuited vias.

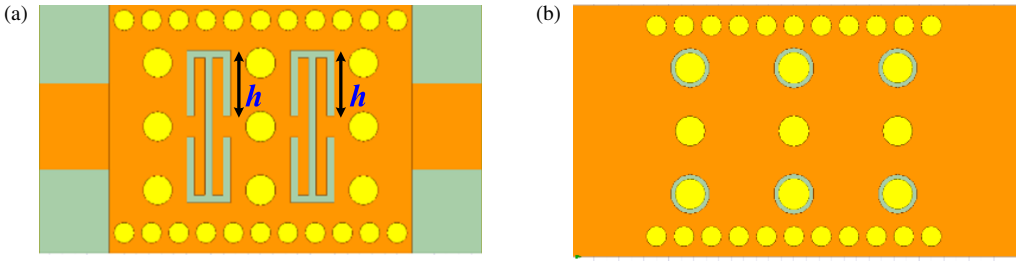

FIGURE 30. Double-slot SIW bandpass filter using the short- and open-circuited vias. (a) Top view. (b) Bottom view.

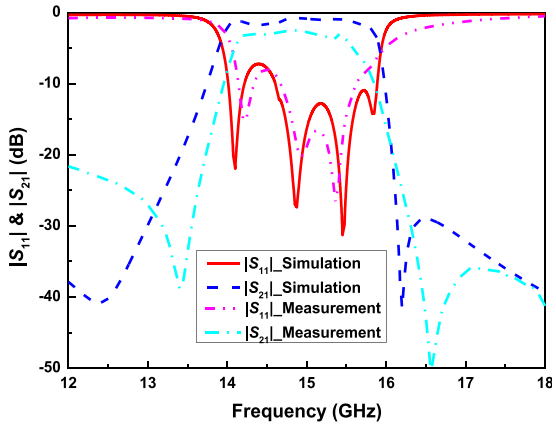

FIGURE 31. Comparison between the simulated and measured frequency responses of the reflection and transmission coefficients for the double-slot SIW bandpass filter using the short- and open-circuited vias.

4. DOUBLE-SLOT SIW BANDPASS FILTER USING SHORT- AND OPEN-CIRCUITED VIAS

4.1. Circuit Implementation and Analysis

To enhance out-of-band suppression, two single-slot structures shown in Fig. 24(a) are integrated with the SIW bandpass filter using the short- and open-circuited vias shown in Fig. 18, and a double-slot SIW bandpass filter using the short- and open-circuited vias can be realized as shown in Fig. 30. The slot is located in the quarter-wavelength SIW portion of the filter, eliminating the need to increase circuit area. The dimensions of the double slots are listed in Table 2. An HFSS simulation of the double-slot SIW bandpass filter using the short- and open-circuited vias in Fig. 30 was performed, and the frequency responses of reflection and transmission coefficients are shown in Fig. 31. As can be seen from Fig. 31, the double-slot structure enhances the suppression depth of the transmission coefficient around 16.2 GHz, achieving $|S_{21}|$ below -30 dB. As compared

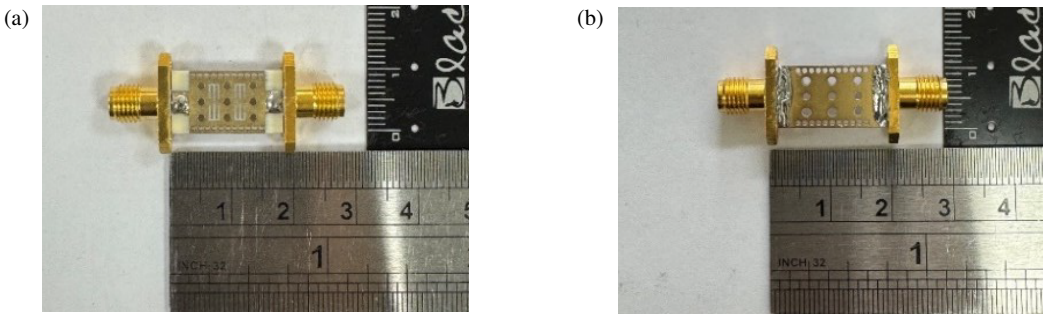

FIGURE 32. Real circuit of the double-slot SIW bandpass filter using the short- and open-circuited vias. (a) Top view. (b) Bottom view.

TABLE 3. Comparison of SIW filters using various techniques.

SIW Filter Using		Frequency Band	3 dB BW (%)	Max IL (dB)	RL (dB)	Max Stopband rejection (dB)	Size ($\lambda_g \times \lambda_g$)
Coupled Slots [9]		Ku	3.93/3.47%	$< 1.15/1.45$	$> 27/25$	None	1.95×0.97
Defected Microstrip Slot [10]		Ku/K	4.39/10.1/7.9%	< 0.6	> 20	None	1.95×0.97
Cavity [11]		X	8.3%	< 2	> 10	None	2.83×0.71
Mushroom-Shaped Resonators [14]		C	4.65%	< 5	> 20	> 60	1.39×0.64
Defected Ground Structure [16]		Ka	26.92%	< 2	> 10	> 30	2.02×0.76
E-Shaped Defected Ground Structure [19]		C	5.8/6.45%	< 3.6	> 15	> 35	0.2×0.2
SC and OC Vias	Simulation	Ku	13%	< 1.5	> 10	None	1.04×0.71
	Measurement	Ku	9.82%	< 3	> 10	None	1.04×0.71
SC and OC Vias with Single-Slot	Simulation	Ku	13.08%	< 2	> 10	> 20	1.04×0.71
	Measurement	Ku	9.82%	< 5	> 10	> 20	1.04×0.71
SC and OC Vias with Double-Slot	**Simulation**	**Ku**	**13.47%**	$\mathbf{< 2}$	$\mathbf{> 10}$	$\mathbf{> 50}$	$\mathbf{1.04 \times 0.71}$
	Measurement	Ku	9.82%	< 5	> 10	> 30	1.04×0.71

with the transmission coefficient for the single-slot SIW bandpass filter using the short- and open-circuited vias in Fig. 27, the transmission coefficient around 16.2 GHz is reduced from -20 dB to -30 dB.

4.2. Implementation and Measurement Results

To verify the performance of the double-slot SIW bandpass filter using short- and open-circuited vias, the double-slot SIW bandpass filter using the short- and open-circuited vias in Fig. 30 is fabricated as shown in Fig. 32. To facilitate measurement, SMA connectors were soldered to the microstrip input/output ports. After calibrating a vector network analyzer (Agilent E5071C) using the Keysight 85521A calibration kit, S-parameters were measured and compared with HFSS simulation results. A comparison of the simulated and measured results is shown in Fig. 31. The measurement results agree well with the simulation ones. The measured reflection coefficient $|S_{11}|$ remains below -10 dB within the passband, indicating good impedance matching. The measured transmission coefficient $|S_{21}|$ also exhibits multi-resonance characteristics of the third-order bandpass filter. However, the measured $|S_{21}|$ is slightly lower than the simulated $|S_{21}|$, which is likely due to the losses introduced by SMA connectors. Regarding the high-frequency notch, the simulation result predicts a notch frequency of 16.2 GHz, while the measured notch frequency shifts slightly to around 16.5 GHz, primarily due to manufacturing etching errors. Nevertheless, the double-slot structure demonstrates superior notch suppression compared to the single-slot structure, with a minimum $|S_{21}|$ below 30 dB.

5. CONCLUSION

This paper proposes a compact substrate-integrated waveguide (SIW) bandpass filter with transmission zeros. First, a SIW bandpass filter using the short- and open-circuited vias was realized. The filter has a passband range of 14.15 GHz to 15.86 GHz and a reflection loss $|S_{11}|$ below -10 dB, demonstrating good matching and passband performance. To enhance the filter's out-of-band suppression, a single-slot structure is introduced within the quarter-wavelength SIW segment. Since the single-slot structure is implemented within the quarter-wavelength SIW segment, no additional circuit area is required. The single-slot SIW bandpass filter using short- and open-circuited vias produces a transmission zero at 16.5 GHz with an insertion loss below -20 dB. To further enhance the filter's out-of-band suppression, a double-slot structure is introduced within the quarter-wavelength SIW segment, creating a deeper

zero at the same frequency and significantly improving stopband rejection while maintaining the original passband characteristics. The insertion loss at the 16.5 GHz transmission zero is below −30 dB for the double-slot SIW bandpass filter using short- and open-circuited vias. This design offers advantages such as high selectivity, compact size, and a simple structure, making it suitable for filtering applications that require transmission zeros in high-frequency communications and radar systems. To verify the accuracy of the design, three filters were fabricated and measured: a SIW bandpass filter using short- and open-circuited vias, a single-slot SIW bandpass filter using short- and open-circuited vias, and a double-slot SIW bandpass filter using short- and open-circuited vias. The measured results agree well with the simulated ones, confirming the accuracy of the design. Table 3 compares the SIW filters using various techniques; among them, the double-slot SIW bandpass filter, which utilizes short- and open-circuited vias, exhibits good performance.

ACKNOWLEDGEMENT

This work was supported in part by the National Science and Technology Council, Taiwan, under Grant NSTC 114-2221-E-011-075. The authors would like to thank Wireless Communications & Applied Electromagnetic Laboratory, National Taiwan University of Science and Technology, Taipei, Taiwan, for providing the simulation environment and measurement instruments.

REFERENCES

[1] Thomson, J. J., *Notes on Recent Researches in Electricity and Magnetism*, 344–347, 1893 (reprinted London: Dawsons, 1968).

[2] Packard, K. S., "The origin of waveguides: A case of multiple rediscovery," *IEEE Transactions on Microwave Theory and Techniques*, Vol. 32, No. 9, 961–969, Sep. 1984.

[3] Guo, J., T. Djerafi, and K. Wu, "Mode composite waveguide," *IEEE Transactions on Microwave Theory and Techniques*, Vol. 64, No. 10, 3187–3197, Oct. 2016.

[4] Grieg, D. D. and H. F. Engelmann, "Microstrip — A new transmission technique for the klilomegacycle range," *Proceedings of the IRE*, Vol. 40, No. 12, 1644–1650, Dec. 1952.

[5] Wen, C. P., "Coplanar waveguide, a surface strip transmission line suitable for nonreciprocal gyromagnetic device applications," in *1969 G-MTT International Microwave Symposium*, 110–115, Dallas, TX, USA, 1969.

[6] Mariani, E. A., C. P. Heinzman, J. P. Agrios, and S. B. Cohn, "Slot line characteristics," *IEEE Transactions on Microwave Theory and Techniques*, Vol. 17, No. 12, 1091–1096, Dec. 1969.

[7] Uchimura, H., T. Takenoshita, and M. Fujii, "Development of a "laminated waveguide"," *IEEE Transactions on Microwave Theory and Techniques*, Vol. 46, No. 12, 2438–2443, Jan. 1998.

[8] Deslandes, D. and K. Wu, "Design consideration and performance analysis of substrate integrated waveguide components," in *2002 32nd European Microwave Conference*, 1–4, Milan, Italy, 2002.

[9] Paliwal, R., R. Budhiraja, S. Srivastava, and S. Yadav, "Design of compact double pass band SIW filter using coupled slot for Ku band application," in *2021 IEEE Indian Conference on Antennas and Propagation (InCAP)*, 855–858, Jaipur, Rajasthan, India, 2021.

[10] Paliwal, R. and R. Budhiraja, "Design of substrate integrated waveguide based triple band pass filter for Ku and K band application," in *2022 8th International Conference on Signal Processing and Communication (ICSC)*, 97–101, Noida, India, 2022.

[11] George, J. M. and S. Raghavan, "A design of miniaturized SIW-based band-pass cavity filter," in *2017 International Conference on Communication and Signal Processing (ICCSP)*, 622–624, Chennai, India, 2017.

[12] Sdobnova, V. P., S. V. Krutiev, A. S. Makhno, and D. V. Lonkina, "Compact band-pass filter made using SIW technology," in *2023 Radiation and Scattering of Electromagnetic Waves (RSEMW)*, 36–39, Divnomorskoe, Russian Federation, 2023.

[13] Goldfarb, M. E. and R. A. Pucel, "Modeling via hole grounds in microstrip," *IEEE Microwave and Guided Wave Letters*, Vol. 1, No. 6, 135–137, Jun. 1991.

[14] Tomassoni, C., L. Silvestri, M. Bozzi, and L. Perregrini, "Quasi-elliptic SIW band-pass filter based on mushroom-shaped resonators," in *2015 European Microwave Conference (EuMC)*, 749–752, Paris, France, 2015.

[15] Parameswaran, A. and S. Raghavan, "Band stop filter in SIW using partial height via," in *2018 IEEE Indian Conference on Antennas and Propogation (InCAP)*, 1–4, Hyderabad, India, 2018.

[16] Chu, S., "Design of a SIW wide-band bandpass filter loaded by DGS," in *2021 IEEE International Conference on Emergency Science and Information Technology (ICESIT)*, 746–749, Chongqing, China, 2021.

[17] Cao, W., Z. Zhang, S. Li, and P. Liu, "Ka band band-stop filter based on complementary split ring and SIW resonators," in *2016 11th International Symposium on Antennas, Propagation and EM Theory (ISAPE)*, 832–833, Guilin, China, 2016.

[18] Souri, M., N. Masoumi, M. Mohammad-Taheri, and S. Karimian, "A dual stopband SIW Ka-V band filter," in *2019 27th Iranian Conference on Electrical Engineering (ICEE)*, 437–441, Yazd, Iran, 2019.

[19] Xu, S., K. Ma, F. Meng, and K. S. Yeo, "Novel defected ground structure and two-side loading scheme for miniaturized dual-band SIW bandpass filter designs," *IEEE Microwave and Wireless Components Letters*, Vol. 25, No. 4, 217–219, Apr. 2015.

[20] Pozar, D. M., *Microwave Engineering: Theory and Techniques*, 2nd ed., John Wiley & Sons, New York, 1998.